arXiv:1210.5504v2 [cond-mat.supr-con] 10 Dec 2012

Uniaxial stress effects on the structural and electronic properties of $BaFe_2As_2$ and $CaFe_2As_2$

Milan Tomić, Harald O. Jeschke, and Roser Valentí
Institut für Theoretische Physik, Goethe-Universität Frankfurt,
Max-von-Laue-Straße 1, 60438 Frankfurt am Main, Germany

(Dated: December 11, 2012)

Starting from the orthorhombic magnetically ordered phase, we investigate the effects of uniaxial tensile and compressive stresses along **a**, **b**, and the diagonal **a**+**b** directions in $BaFe_2As_2$ and $CaFe_2As_2$ in the framework of *ab initio* density functional theory (DFT) calculations. While –contrary to the application of hydrostatic or *c*-axis uniaxial pressure– both systems remain in the orthorhombic phase with a pressure-dependent nonzero magnetic moment, we observe an inversion of magnetism at a critical pressure happening when the *a* and *b* axes approach the tetragonal condition. Moreover, this is followed by a jump in orthorhombicity as well as a selective change of orbital occupancy. We estimate elastic constants and discuss our results in view of recent reports of modified magnetic and structural transitions in $BaFe_2As_2$ under externally applied uniaxial stress and some proposed phenomenological models.

PACS numbers: 74.70.Xa,61.50.Ks,71.15.Mb,64.70.K-

INTRODUCTION

Since the discovery of high-Tc superconductivity in Fe-based materials in 2008, [1] an enormous amount of effort has been invested to understand the microscopic behavior of these materials. Iron pnictides and chalcogenides become superconductors either by hole- or electron-doping the systems, by application of external pressure or by a combination of both. In particular, uniaxial pressure is currently being intensively discussed as a possible route towards modifying the structural, magnetic and even superconducting properties of these systems. Uniaxial tensile stress was initially applied to bilayer Fe pnictides like $BaFe_2As_2$ in order to detwin the crystals. [2–5] Recent neutron scattering experiments on $BaFe_2As_2$ under compressive stress along the in-plane **b** direction reported a progressive shift to higher temperatures of both the tetragonal-to-orthorhombic phase transition as well as the magnetic transition. [6] Also, Blomberg *et al.* observed a significant uniaxial structural distortion in $BaFe_2As_2$ under tensile stress. [7] More recently, it was found that epitaxially strained thin films of FeSe on a $SrTiO_3$ substrate show an increase in critical superconducting temperatures up to 65 K, the highest reported T_c so far. [8] Clearly, crystal lattice strain plays a key role for the magnetic, structural and superconducting properties in Fe-based superconductors and a better understanding of the microscopic origin of such behavior is desirable.

In this work we analyze by means of density functional theory (DFT) calculations the effects of uniaxial compressive stress as well as uniaxial tensile stress on the magnetic, electronic and structural properties of $BaFe_2As_2$ and $CaFe_2As_2$ at low temperatures. We measure stress in terms of equivalent hydrostatic pressure, $P = \mathrm{Tr}(\hat{\boldsymbol{\sigma}})/3$, where $\hat{\boldsymbol{\sigma}}$ is the stress tensor matrix and positive and negative pressures correspond to applying compressive and tensile stresses respectively. While no sign of a true structural or magnetic phase transition is observed in the range of pressures between -2 GPa and 2 GPa, there is an inversion in the magnetization, i.e. exchange of ferromagnetic (FM) and antiferromagnetic (AFM) directions, at the stresses where *a* and *b* reach the tetragonal condition *a*=*b*. Interestingly, $CaFe_2As_2$ shows these effects at larger pressures than $BaFe_2As_2$. This has also important consequences on the orbital d_{xz} and d_{yz} occupancies and should manifest in a shift of the magnetic ordering temperature as we shall discuss below. Our results support recent suggestions [9] that a shift in the magnetic ordering temperature T_{N} should be observed under application of stress and we provide in this context *ab initio*-derived estimates for the elastic constants. Also, a sharp orthorhombic to tetragonal phase transition is observed for $CaFe_2As_2$ when compressive stress of 7.7 GPa is applied along **a**+**b**.

COMPUTATIONAL METHODS

Electronic structure calculations were performed within DFT with the Vienna ab initio simulations package (VASP) [10] with the projector augmented wave (PAW) basis [11] in the generalized gradient approximation (GGA). All our structural relaxations were performed under constant stress using the Fast Inertial Relaxation Engine (FIRE) [12, 13]. For this purpose, we had to modify the algorithm accordingly (see Appendix). Every 10 steps, we cycled through non-magnetic, ferromagnetic, antiferromagnetic-checkerboard, stripe-type antiferromagnetic (along unit cell axis **a**) and stripe-type antiferromagnetic (along unit cell axis **b**) spin configurations, and then we continued the relaxation with the lowest energy spin configuration. As a final converged magnetic configuration in the orthorhombic phase we had always found stripe-type antiferromagnetic order either along **a** or along **b**, as discussed below.

The energy cutoff in the calculations was set to 300 eV and a Monkhorst-Pack uniform grid of $(6 \times 6 \times 6)$ points was used for the integration of the irreducible Brillouin zone (BZ).

RESULTS AND DISCUSSION

$BaFe_2As_2$

Starting from the low-temperature orthorhombic structure with stripe magnetic order, we performed structure relaxations under applied uniaxial tensile and compressive stresses along **a** (AFM direction), **b** (FM direction) and the plane-diagonal **a**+**b** for both $BaFe_2As_2$ and $CaFe_2As_2$. We simulated pressures in the range between -3 GPa and 3 GPa. In the tensile stress range, below -2.7 GPa we observe in both systems that for stress along **a**, a sudden expansion in a and contraction in b and c axes occurs, and analogously (with a change of axes) a similar situation arises when pulling apart along **b**. This feature signals the extreme case of absence of bonding within the material, and this pressure range will be excluded from further discussion.

Fig. 1 shows the evolution of lattice parameters for $BaFe_2As_2$ as a function of uniaxial stress along **a**, **b** and **a**+**b**. At $P = 0$ GPa a (AFM direction) $> b$ (FM direction). $BaFe_2As_2$ remains in the orthorhombic phase with nonzero increasing magnetic moment for large tensile stress (negative pressure). Pulling apart along the (longer) AFM direction **a** (Fig. 1 (a)) the system expands along **a**, strongly compresses along **c** and shows almost no changes along **b**; similarly, pulling apart along the (shorter) FM direction **b** (Fig. 1 (b)) b expands, c compresses and a shows almost no changes except for a pressure $P = -0.22$ GPa (Fig. 1 (e)). In this case, $a \approx b$ and $BaFe_2As_2$ shows a sudden jump in orthorhombicity where **a** becomes the shorter axis and **b** becomes the longer axis. This interchange happens with a rotation of the magnetic order by 90 degrees. Now, the FM direction is along the **a** axis and the AFM direction is along the **b** axis. We will discuss this feature below.

Tensile stress along **a**+**b** acts similarly on both **a** and **b** directions, which expand, while the **c** direction strongly compresses (Fig. 1 (c) and (f)).

Under application of compressive stress (positive pressure), we observe in all three cases a strong expansion along **c**, a compression along the direction of applied stress; **a**, **b** or **a**+**b**, and almost no changes or a slight expansion along **b** and **a** for the first two cases, respectively. A slight expansion along **a** has also been measured upon application of uniaxial stress along **b** by Dhital *et al.* [6]. $BaFe_2As_2$ remains in all cases orthorhombic with nonzero decreasing magnetic moment. Since $a > b$ at zero stress, we observe the inversion of axes followed by a jump in orthorhombicity and a 90 degree rotation of the magnetization when stress is applied along **a** at $P = 0.22$ GPa (Fig. 1 (a) and (d)). This inversion of axes, with $b > a$ for all higher compressive stress values means that the spin configuration shown in the inset of Fig. 1 (a) should now be turned by 90 degrees, with **b** pointing along the AFM direction. Such an inversion is also observed for compressive stress along **a**+**b** at much larger pressures of $P = 2$ GPa.

Fig. 2 shows the evolution of magnetic moment, volume and As height in $BaFe_2As_2$ as a function of stress. The three quantities show a clearly monotonic behavior independent of the applied stress direction except for small jumps at the pressures $P = -0.22$ GPa (for stress along **a**) and $P = 0.22$ GPa (for stress along **b**) where the tetragonal condition is almost fulfilled ($a \approx b$) (Fig. 2 (b), (d), (f)). Even though DFT calculations overestimate the value of the ordered Fe magnetic moment at $P = 0$ GPa, it is to be expected that the relative changes in magnetic moment should provide a reliable description of the situation of $BaFe_2As_2$ under pressure effects as shown in previous studies [13–16].

Except for the pressures $P = -0.22$ GPa (for stress along **a**) and $P = 0.22$ GPa (for stress along **b**), stress always enforces a certain degree of orthorhombicity and the system remains magnetically ordered with a decreasing ordered moment as a function of compressive stress (Fig. 2 (a)). Moreover, since the c axis continually expands from negative to positive pressures, h_{As} increases accordingly as a function of stress (Fig. 2 (e)). These features have a direct consequence on the electronic properties of the system.

As an illustration, we show the evolution of the Fermi surface of $BaFe_2As_2$ under application of uniaxial stress applied along **a** in Fig. 3 in the 1Fe/unit cell equivalent Brillouin zone. At ambient pressure conditions (Fig. 3 (b)) we observe three hole pockets centered around $\bar{\Gamma}$ and $\bar{M}$ and two electron pockets centered around $\bar{X}$. Application of modest tensile stress of 0.07 GPa leads to the disappearance of the $3d_{xy}$ hole pocket around $\bar{\Gamma}$ in the $k_z = 0$ plane (Fig. 3 (a) and (b)). On the other hand, when compressive stress is applied, the $3d_{xy}$ hole pocket around $\bar{\Gamma}$ significantly increases in size, and additionally, at a pressure of 1.7 GPa, small electron pockets, of majority $3d_{xy}$ and $3d_{z^2}$ character, appear along the $\bar{\Gamma} - \bar{M}$ directions of the BZ (Fig. 3 (c) and (e)). The increase of the $3d_{xy}$ hole pocket size with increasing uniaxial stress can be explained by the reduction of Fe-Fe distance along the **a** axis, leading to an increased contribution of $3d_{xy}$ - $3d_{xy}$ bonding. In fact, the effects of tensile and compressive stress on the electronic structure shown for the example of stress along **a** can be seen also in our calculations for both stress along **b** and along **a**+**b**.

A more detailed information of the orbital occupation

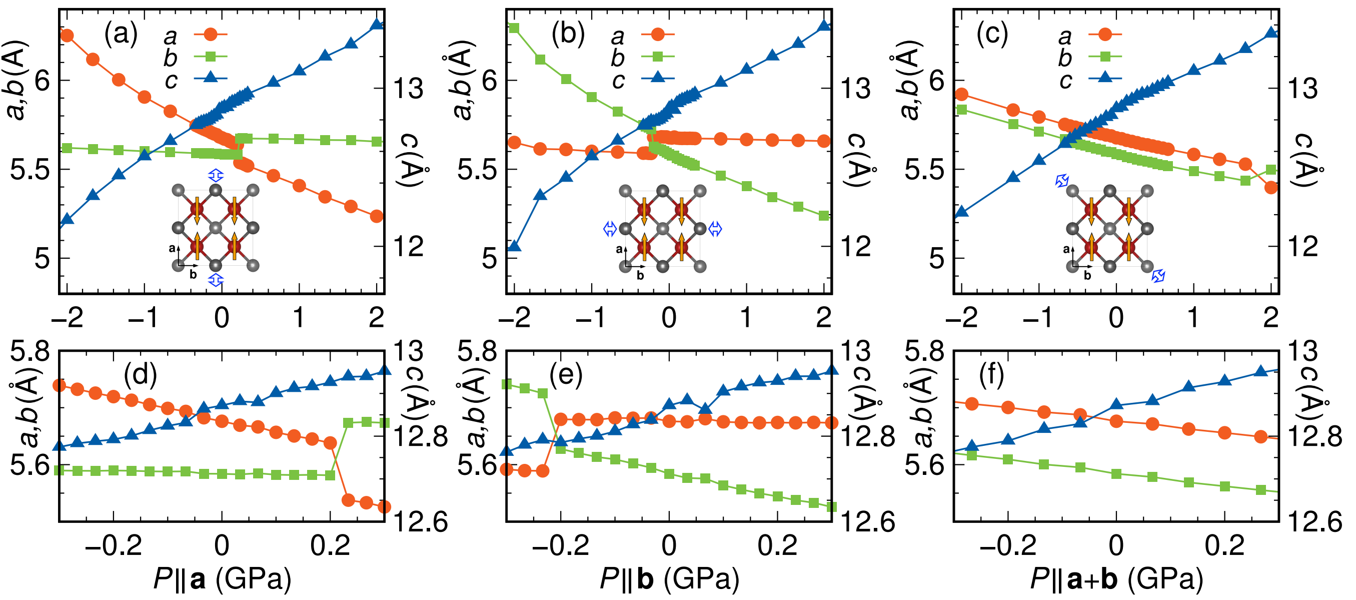

FIG. 1: (Color online) Evolution of the unit cell parameters in $BaFe_2As_2$ under application of uniaxial stress in the equivalent hydrostatic pressure range $[-2\,\mathrm{GPa}, 2\,\mathrm{GPa}]$ (a) along **a**, (b) along **b** and (c) along **a**+**b**. Panels (d)-(f) show a corresponding blow-up of the pressure dependence of the lattice parameters in the range $[-0.3\,\mathrm{GPa}, 0.3\,\mathrm{GPa}]$. Negative pressures correspond to tensile stress while positive pressures correspond to compressive stress. Note, that the relationship between axes and iron moments shown in the inset in (a) is valid for $P \parallel \mathbf{a} < 0.22$ GPa, in (b) for $P \parallel \mathbf{b} > -0.22$ GPa. For a discussion of the reversal of AFM order, see the text.

can be obtained by analyzing the density of states at the Fermi level $N(E_\mathrm{F})$. Applying stress both along **a** and **b** has the same effect on the total density of states of both $BaFe_2As_2$ and $CaFe_2As_2$, but there is a selective orbital order as shown in Fig. 4. $N(E_\mathrm{F})$ is predominantly of $3d_{xz}$ character when $a > b$ and of $3d_{yz}$ character when $a < b$. This means that the dominant character switches from $3d_{yz}$ to $3d_{xz}$ at $\hat{\boldsymbol{\sigma}} \parallel \mathbf{a} \approx 0.22$ GPa, and from $3d_{xz}$ to $3d_{yz}$ at $\hat{\boldsymbol{\sigma}} \parallel \mathbf{b} \approx -0.22$ GPa as expected.

Clearly, approaching or moving away from the tetragonal situation a=b by applying external stress will have important consequences on the magnetic phase transition temperature T_N. T_N will shift to higher temperatures the further away the system is from the tetragonal situation. If we consider, f.i., application of tensile stress along **a** (longer direction), the degree of orthorhombicity increases and T_N should increase. On the contrary, by applying compressive stress along **a** up to pressures where $a \approx b$, we expect a shift of T_N to lower temperatures. This is in agreement with a recent proposal that predicts a shift in T_N as a function of stress based on a phenomenological model [9, 17].

$\mathbf{CaFe_2As_2}$

The lattice parameters of $CaFe_2As_2$ under application of compressive stress along **a**, **b** and **a**+**b** directions show a similar overall behavior compared to $BaFe_2As_2$ (see Fig. 5) except for some important shifts of the pressures at which the system exchanges the FM by the AFM directions. When stress is applied along the **a** direction, we observe at $P = 0.67$ GPa a compression of the unit cell to the tetragonal symmetry. However, analogously to the case of $BaFe_2As_2$, this is not followed by the suppression of the magnetic moments of iron. In fact, the c axis expands through the stress application and at $P = 0.67$ GPa the c lattice parameter in $CaFe_2As_2$ is too large for the formation of an interlayer As-As covalent bond, necessary for a transition to a collapsed tetragonal phase and suppression of magnetic moments as observed under hydrostatic or c-axis uniaxial pressure. [13–15, 18]

For tensile stress along the (shorter) **b** direction, the inversion of axes happens at $P = -0.33$ GPa followed by a jump in the orthorhombicity.

In order to investigate the possibility of a structural and/or magnetic phase transition at higher pressures, we concentrate now on compressive stress along the diagonal of the ab-plane. We find that orthorhombicity is preserved up to 7.7 GPa, where a sharp transition to a tetragonal phase appears. This transition is of first-order type like the orthorhombic to collapsed tetragonal phase transition under application of hydrostatic or uniaxial pressure along the **c** axis [13] but in this case, changes of magnetic and structural properties take opposite directions; the **c** axis undergoes a sudden expansion of about

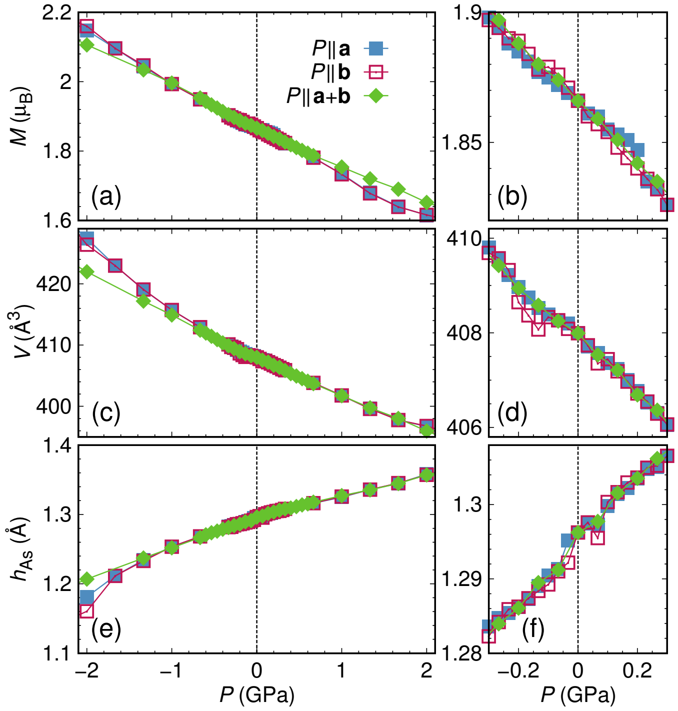

FIG. 2: (Color online) (a) Evolution of the magnetic moments of iron, (c) of the unit cell volume and (e) of the pnictogen height under uniaxial pressure in the range $[-2\,\text{GPa}, 2\,\text{GPa}]$. Panels (b), (d) and (e) show the corresponding blow-up of the pressure dependence of these quantities in the range $[-0.3\,\text{GPa}, 0.3\,\text{GPa}]$. Negative pressures correspond to tensile stress while positive pressures correspond to compressive stress.

9.5%, and **a** and **b** axes contract while the iron magnetic moments order ferromagneticaly and sharply increase in value by around 25%. Interestingly though, contrary to the application of hydrostatic and uniaxial pressure along **c** axis, the volume change here is significantly smaller, namely an expansion by about 0.9%.

ELASTIC PROPERTIES

Utilizing data for the response to the uniaxial stress along **a**, **b** and **c** [13] axes we can directly evaluate elastic constants C_{ij} in $BaFe_2As_2$ and $CaFe_2As_2$ corresponding to the orthorhombic deformations. We define elastic constants to be such that

$$\sigma_i = \sum_j C_{ij} u_j ,$$

where σ_i and u_j are stress and strain tensor components respectively, and indices i and j can be xx, yy, zz. Strains are defined to be $u_{xx} = (a-a_0)/a_0$, $u_{yy} = (b-b_0)/b_0$ and $u_{zz} = (c-c_0)/c_0$, where a_0, b_0 and c_0 are equilibrium unit cell dimensions ($P = 0$ GPa). We first directly obtain $S_{ij} = [C^{-1}]_{ij}$ by performing linear fits to $u_i(\sigma_j)$ and C is then obtained by inverting the resulting matrix. For $BaFe_2As_2$, the elastic constant matrix is

$$C = \begin{bmatrix} 95.2 \pm 4.3 & 20.4 \pm 3.4 & 40.8 \pm 4.5 \\ 27.3 \pm 4.8 & 130.8 \pm 6.1 & 64.0 \pm 7.0 \\ 43.7 \pm 4.5 & 47.7 \pm 4.6 & 81.0 \pm 5.6 \end{bmatrix} \text{GPa} \quad (1)$$

Utilizing Voigt and Reuss averages [19], defined as

$$B_{\text{Voigt}} = \frac{1}{9}(C_{11} + C_{22} + C_{33} + 2(C_{12} + C_{13} + C_{23}))$$
$$B_{\text{Reuss}} = (S_{11} + S_{22} + S_{33} + 2(S_{12} + S_{13} + S_{13}))^{-1}$$

it is possible to estimate the bulk modulus. Voigt and Reuss averages yield 61.9 ± 5.1 GPa and 69.3 ± 7.5 GPa, respectively, which is in good agreement with our previous estimate [13] and the experimental value of 59 ± 2 GPa [20]. For $CaFe_2As_2$, the elastic constant matrix is given by

$$C = \begin{bmatrix} 148.7 \pm 18.5 & 45.6 \pm 12.3 & 55.5 \pm 12.7 \\ 63.9 \pm 21.4 & 182.4 \pm 18.4 & 81.2 \pm 17.5 \\ 61.4 \pm 14.7 & 63.1 \pm 11.4 & 68.8 \pm 11.3 \end{bmatrix} \text{GPa} \quad (2)$$

which results in bulk modulus of 84.3 ± 14.8 GPa and 77.7 ± 17.2 GPa using Voigt and Reuss averages, respectively. Both values are in good agreement with experimentally determined values of 82.9 ± 1.4 GPa [21] and the estimate based on fits to Birch-Murnaghan equation of state [13].

CONCLUSIONS

In summary, we analyzed the effects of tensile and compressive stress along **a**, **b** and **a**+**b** on $BaFe_2As_2$ and $CaFe_2As_2$ by means of DFT calculations under constant stress conditions with the help of the FIRE algorithm. Starting from the low-temperature magnetically ordered orthorhombic phase, we find in the pressure range between −2 GPa and 2 GPa no real structural phase transitions in both systems except for a pronounced orthorhombicity jump in the region where $a \approx b$ accompanied by a 90 degree rotation of the magnetic order. FM and AFM directions are interchanged, as are the orbital occupations d_{xz} and d_{yz}. This inversion of axes is purely of magnetoelastic origin. This phenomenon should be observable experimentally. Moreover, we also find a slight expansion along the **a** axis when compressive stress is applied along **b** in $BaFe_2As_2$, as reported recently [6]. Our results agree with recent phenomenological theories predicting a shift in T_N depending on the stress conditions. Finally we provide estimates for the elastic constants of $BaFe_2As_2$ and $CaFe_2As_2$. The Bulk moduli calculated with these estimates are in good agreement with the experimental measurements.

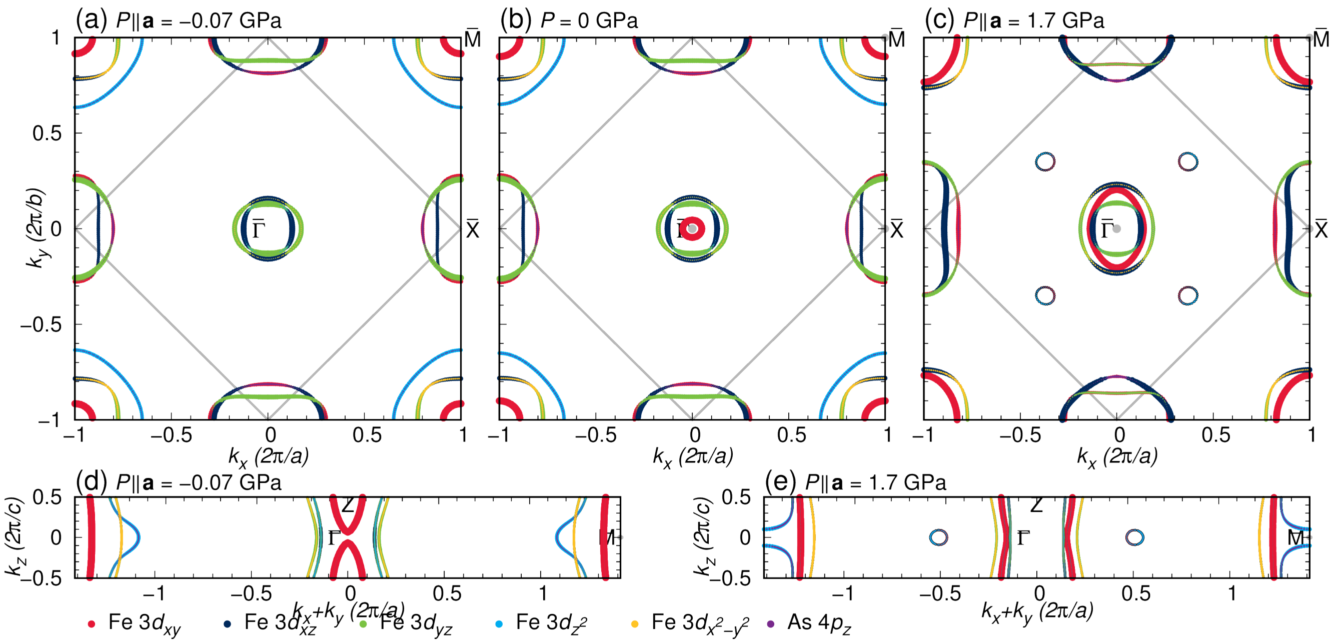

FIG. 3: (Color online) Evolution of the Fermi surface of $BaFe_2As_2$ under uniaxial stress applied along the **a** axis shown in the 1Fe/unit cell equivalent BZ (see [22] for the BZ path definition). Panels (a), (b) and (c) show $k_z = 0$ cuts of the Fermi surface at pressures of -0.07 GPa, 0 GPa and 1.7 GPa respectively, while panels (d) and (e) show vertical cuts along the diagonal of the BZ for pressures of -0.07 GPa and 1.7 GPa. Grey lines on panels (a), (b) and (c) denote boundaries of the 2 Fe/unit cell BZ.

APPENDIX A

Within the FIRE [12] algorithm, the energy minimization is achieved by moving the system's position $\boldsymbol{r}$ according to the following equation of motion:

$$\dot{\boldsymbol{v}}(t) = \frac{\boldsymbol{F}(t)}{m} - \gamma(t)|\boldsymbol{v}(t)|\left[\boldsymbol{e}_{\boldsymbol{v}(t)} - \boldsymbol{e}_{\boldsymbol{F}(t)}\right] , \qquad (3)$$

where $\boldsymbol{e}_{\boldsymbol{x}}$ denotes the unit vector along $\boldsymbol{x}$, with $\boldsymbol{x} = \boldsymbol{v}(t), \boldsymbol{F}(t)$, t is time and $\gamma(t)$ is a time-dependent friction parameter which assures that the system is moving down the energy hypersurface in an optimal manner as long as the power $P(t) = \boldsymbol{F}(t)\cdot\boldsymbol{v}(t)$ is positive. If $P(t)$ becomes negative, the procedure is stopped and relaxation is reinitialized in the direction of the steepest descent.

In order to use FIRE for relaxation of periodic systems, we change from the configuration space of $3N$ atomic Cartesian coordinates $\boldsymbol{r}^{\alpha}$, $\alpha = 1 \dots N$, to an extended system of $3N + 9$ coordinates $\tilde{\boldsymbol{r}}^{\alpha} = (\boldsymbol{s}^{\alpha}, \hat{\mathbf{h}})$, consisting of lattice vectors which are contained in columns of the 3×3 matrix $\hat{\mathbf{h}} = (h_{ij})$, and fractional atomic positions $\boldsymbol{s}^{\alpha}$ within the unit cell, where Cartesian and fractional positions are related by $\boldsymbol{r}^{\alpha} = \hat{\mathbf{h}}\boldsymbol{s}^{\alpha}$.

When (3) is rewritten in terms of coordinates $\tilde{\boldsymbol{r}}^{\alpha}$, one just needs to find the appropriate expression for forces $\tilde{\boldsymbol{F}}^{\alpha}$, that is, derivatives of energy with respect to the coordinates $\tilde{\boldsymbol{r}}^{\alpha}$. Since stress and strain tensors, $\hat{\sigma}$ and $\hat{\mathbf{u}}$, can be defined through

$$\hat{\boldsymbol{\sigma}} = -\frac{1}{V}\frac{\partial E}{\partial \hat{\mathbf{u}}}, \qquad \hat{\mathbf{H}} = \left(\hat{\mathbf{I}} + \hat{\mathbf{u}}\right)\hat{\mathbf{h}},$$

where $\hat{\mathbf{I}}$ is the identity matrix and $\hat{\mathbf{H}}$ is the lattice matrix after an infinitesimal deformation, it is easy to show that

$$\begin{aligned} \frac{\partial E}{\partial \boldsymbol{s}^{\alpha}} &= \sum_{\beta} \frac{\partial E}{\partial \boldsymbol{r}^{\beta}} \frac{\partial \boldsymbol{r}^{\beta}}{\partial \boldsymbol{s}^{\alpha}} = \frac{\partial E}{\partial \boldsymbol{r}^{\alpha}} \hat{\mathbf{h}}^{T} = \boldsymbol{F}^{\alpha} \hat{\mathbf{h}}^{T}, \\ \frac{\partial E}{\partial \hat{\mathbf{h}}} &= \frac{\partial E}{\partial \hat{\mathbf{u}}} \frac{\partial \hat{\mathbf{u}}}{\partial \hat{\mathbf{h}}} = \frac{\partial E}{\partial \hat{\mathbf{u}}} \left(\hat{\mathbf{h}}^{T}\right)^{-1} = -V\hat{\boldsymbol{\sigma}}\left(\hat{\mathbf{h}}^{T}\right)^{-1}, \end{aligned} \qquad (4)$$

so that forces in the extended coordinates are given by

$$\tilde{\boldsymbol{F}}^{\alpha} = \left[\boldsymbol{F}^{\alpha}\hat{\mathbf{h}}^{T}, -V\hat{\boldsymbol{\sigma}}\left(\hat{\mathbf{h}}^{T}\right)^{-1}\right]. \qquad (5)$$

Forces $\boldsymbol{F}^{\alpha}$ and stresses $\hat{\boldsymbol{\sigma}}$ are obtained from the electronic structure code, and are inserted directly into Eq. (5), taking into account that $\hat{\boldsymbol{\sigma}} = \hat{\boldsymbol{\sigma}}^{ext} - \hat{\boldsymbol{\sigma}}^{int}$, that is, total stress is the sum of internal and external stresses applied to the surface of the unit cell.

Acknowledgments.- We would like to thank R. Fernandes for useful discussions and the Deutsche Forschungsgemeinschaft for financial support through grant SPP 1458, the Helmholtz Association for support through HA216/EMMI and the centre for scientific computing (CSC, LOEWE-CSC) in Frankfurt for computing

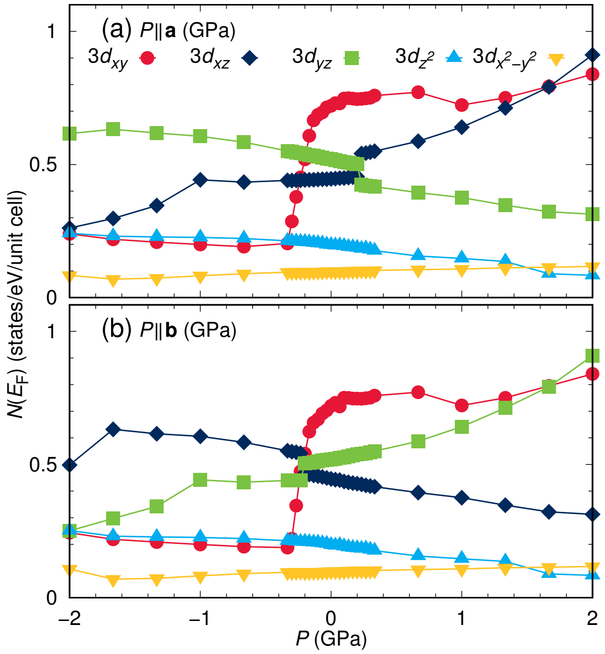

FIG. 4: (Color online) Evolution of the orbital resolved density of states of $BaFe_2As_2$ at the Fermi level $N(E_\mathrm{F})$ with stress (a) applied along **a**, and (b) along **b**. Lines joining the calculated points are a guide for the eye.

facilities. This research was supported in part (RV) by the National Science Foundation under Grant No. NSF PHY11-25915.

[1] Y. Kamihara, T, Watanabe, M, Hirano, H. Hosono, J. Am. Chem. Soc. **130**, 3296 (2008).
[2] J. H. Chu, J. G. Analytis, K De Greeve, P. L. McMahon, Z. Islam, Y. Yamamoto, I. R. Fisher, Science **329**, 824 (2010).
[3] M. A. Tanatar, E. C. Bloomberg, A. Kreyssig, M. G. Kim, N. Ni, A. Thaler, S. L. Bud'ko, P. C. Canfield, A. I. Goldman, I. I. Mazin, R. Prozorov, Phys. Rev. B **81**, 184508 (2010).
[4] H.-H. Kuo, J. H. Chu, S. C. Riggs, L. Yu, P. L. MacMahon, K. De Greeve, Y. Yamamoto, J. G. Analytis, I. R. Fisher, Phys. Rev. B **84**, 054540 (2011).
[5] T. Liang, M. Nakajima, K. Kihou, Y. Tomioka, T. Ito, C. H. Lee, H. Kito, A. Iyo, H. Eisaki, T. Kakeshita, S. Uchida, J. Phys. Chem. Solids **72**, 418 (2011).
[6] C. Dhital, Z. Yamani, W. Tian, J. Zeretsky, A. S. Sefat, Z. Wang, R. J. Birgeneau, S. D. Wilson, Phys. Rev. Lett. **108**, 087001 (2012).
[7] E. C. Blomberg, A. Kreyssig, M. A. Tanatar, R. M. Fernandes, M. G. Kim, A. Thaler, J. Schmalian, S. L. Bud'ko, P. C. Canfield, A. I. Goldman, R. Prozorov, Phys. Rev. B **85**, 144509 (2012).
[8] Q. Y. Wang, Z. Li, W. H. Zhang, Z. C. Zhang, J. S. Zhang, W. Li, H. Ding, Y. B. Ou, P. Deng, K. Chang, J. Wen, C. L. Song, K. He, J. F. Jia, S. H. Ji, Y. Wang, L. Wang, X. Chen, X. Ma, Q.K. Xue, Chin. Phys. Lett. **29**, 037402 (2012).
[9] A. Cano and I. Paul, Phys. Rev. B **85**, 155133 (2012).
[10] G. Kresse and J. Hafner, Phys. Rev. B **47**, 558 (1993); G. Kresse and J. Furthmüller, ibid. **54**, 11169 (1996); Comput. Mater. Sci. **6**, 15 (1996).
[11] P. E. Blöchl, Phys. Rev. B **50**, 17953 (1994); G. Kresse and D. Joubert, ibid. **59**, 1758 (1999).
[12] E. Bitzek , P. Koskinen, F. Gähler, M. Moseler, P. Gumbsch, Phys. Rev. Lett. **97**, 170201 (2006).
[13] M. Tomić, R. Valentí, H. O. Jeschke, Phys. Rev. B **85**, 094105 (2012).
[14] Y.-Z. Zhang, H. C. Kandpal, I. Opahle, H. O. Jeschke, and R. Valentí, Phys. Rev. B **80**, 094530 (2009).
[15] N. Colonna, G. Profeta, A. Continenza, and S. Massidda, Phys. Rev. B **83**, 094529 (2011).
[16] N. Colonna, G. Profeta, and A. Continenza, Phys. Rev. B **83**, 224526 (2011).
[17] J. Hu, C. Setty, and S. Kivelson, Phys. Rev. B **85**, 100507(R) (2012).
[18] A. Kreyssig, M. A. Green, Y. Lee, G D. Samolyuk, P. Zajdel, J. W. Lynn, S. L. Bud'ko, M. S. Torikachvili, N. Ni, S. Nandi, J. B. Leão, S. J. Poulton, D. N. Argyriou, B. N. Harmon, R. J. McQueeney, Phys. Rev. B **78**, 184517 (2008).
[19] J. D. Clayton, *Nonlinear Mechanics of Crystals*, Springer (2010).
[20] J. E. Jørgensen, T. C. Hansen, Eur. Phys. J. B **78**, 411 (2010).
[21] R. Mittal, S. K. Mishra, S. L. Chaplot, S. V. Ovsyannikov, E. Greenberg, D. M. Trots, L. Dubrovinsky, Y. Su, Th. Brueckel, S. Matsuishi, H. Hosono, G. Garbarino, Phys. Rev. B **83**, 054503 (2011).
[22] O. K. Andersen, L. Boeri, Ann. Phys. **523**, 8 (2011).

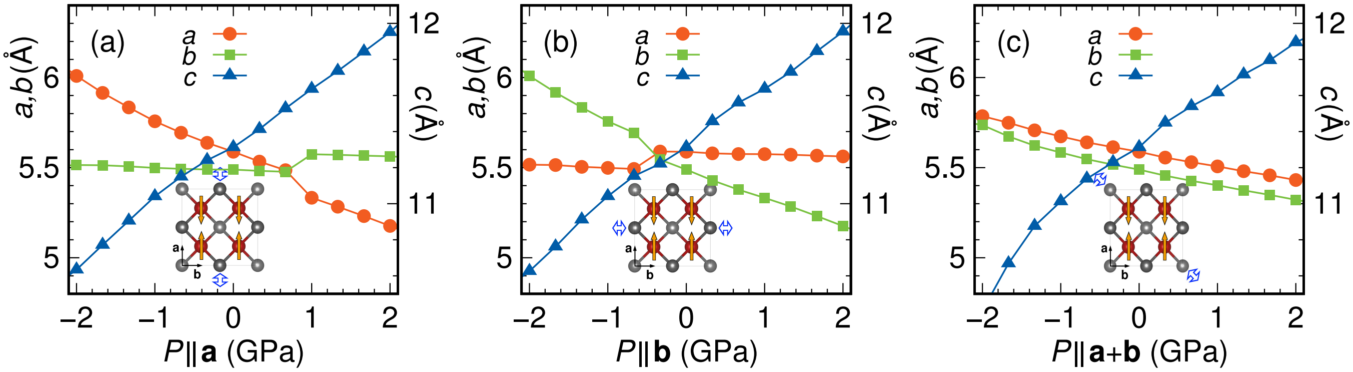

FIG. 5: (Color online) Evolution of the unit cell parameters in $\mathrm{CaFe_2As_2}$ under the application of uniaxial stress in the range $[-2\,\mathrm{GPa}, 2\,\mathrm{GPa}]$ (a) along $\mathbf{a}$, (b) along $\mathbf{b}$ and (c) along $\mathbf{a}+\mathbf{b}$. Negative pressures correspond to tensile stress while positive pressures correspond to compressive stress. Note, that the relationship between axes and iron moments shown in the inset in (a) is valid for $P \parallel \mathbf{a} < 1$ GPa, in (b) for $P \parallel \mathbf{b} > -0.6$ GPa.